Maciej ROSÓŁ, Bogdan SAPIŃSKI
AKADEMIA GÓRNICZO-HUTNICZA, KRAKÓW

Multi-channel power controller for MR dampers of small-scale

Dr inż. Maciej ROSÓŁ

He holds the position of a professor assistant in automatics and robotics in the Department of Automatics, AGH University of Science and Technology in Krakow. Research in the fields of: real-time control systems; distributed control systems using the CAN bus, Ethernet and LonWorks; nonlinear control, microcontroller, PLC and FPGA technology in measurement and control.

e-mail: mr@agh.edu.pl

Prof. dr hab. inż. Bogdan SAPIŃSKI

He holds the position of professor in automatics and robotics in the Department of Process Control, AGH University of Science and Technology in Krakow. Research in the fields of: vibration and motion control, semi-active and active vibration reduction systems, smart materials and structures, application of MR fluids to vibration damping in discrete and continuous mechanical systems, energy harvesting.

e-mail: deep@agh.edu.pl

Abstract

The study deals with the multi-channel power controller engineered by authors for magnetorheological (MR) dampers of small-scale. The paper covers: structure, technical specification, laboratory testing of the device in the analog and digital mode and its testing by applying to MR dampers' control in a vehicle suspension model.

Keywords: power controller, MR damper, vibration control.

Wielokanałowy sterownik mocy dla tłumików MR małej skali

Streszczenie

W artykule przedstawiono opracowany przez autorów, wielokanałowy sterownik mocy dla tłumików MR małej skali (wytwarzających siłę do kilku kN). Opisano budowę oraz podano parametry techniczne sterownika. Omówiono wyniki badań laboratoryjnych sterownika pracującego w trybie analogowym i cyfrowym. Porównano własności statyczne i dynamiczne sterownika w obu trybach, ze szczególnym uwzględnieniem granicznych wartości prądów i napięć na wyjściu sterownika oraz odpowiedzi czasowych na skokowe zmiany sygnałów sterujących (analiza czasów ustalania prądu w cewce sterującej tłumika i siły generowanej przez tłumik MR). Na podstawie wyników badań eksperymentalnych pokazano wady i zalety obu trybów pracy sterownika do sterowania tłumikiem MR, uwzględniając zastosowanie przełączających algorytmów sterowania. Opracowany sterownik wykorzystano do badań płaskiego modelu zawieszenia pojazdu o dwu- i trzech stopniach swobody wyposażonego w tłumiki MR. W badaniach wykorzystano dwa środowiska sprzętowo-programowe: kartę wejść-wyjść AC/CA typu RT-DAC4/PCI i pakiet MATLAB/Simulink z przybornikami RTW/RTWT oraz mikrokontroler Motorola typu MPC 555 z przybornikiem Embedded Target for Motorola® MPC555 pakietu MATLAB/Simulink.

Słowa kluczowe: sterownik mocy, tłumik MR, sterowanie drganiami.

1. Introduction

A conventional MR damper-based vibration reduction system is a system with closed-loop (Fig. 1). Such system includes: sensor(s) − (to detect vibration), controller − (to manipulate the signal obtained from the sensor(s) according to the control law), MR damper(s) − (to control the mechanical response of the structure) and a power controller − to activate MR damper(s). The main function of power controller is to guarantee the required current and voltage range for MR dampers and to ensure the short current response to the preset control signal.

The power controller described in the study was engineered for the purpose of the research program. The device is able to operate in the analog or digital mode.

The study focuses on the structure, technical specification, characteristics and results of laboratory tests of the power controller by applying to MR dampers' control in a vehicle suspension model which was investigated as a structure with two and three degrees of freedom (with 2DOFs and 3DOFs) in the analog and digital mode, respectively.

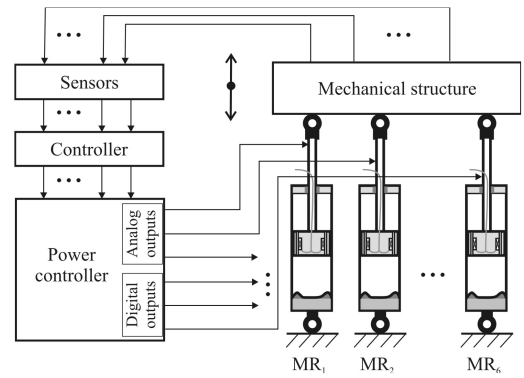

Fig. 1. MR damper-based vibration reduction system
Rys. 1. Układ redukcji drgań z tłumikami MR

2. Power controller

In accordance with the power controller input and output signals we introduced the following designations: in the analog mode; AVI–AVO (voltage input–analog voltage output) and AVI–ACO (analog voltage input–current output), in the digital mode; DVI–DVO (PWM voltage input–PWM voltage output) and DVI–DCO (PWM voltage input–current output).

2.1. Structure and technical specification

A block diagram of a Power controller operating in the analog mode is shown in Fig. 2. The final element is a voltage-controlled power amplifier, equipped with analogue signal conditioning system to allow for setting of the input voltage signal in a fairly broad range (amplification and offset). During tests the power controller was subjected to load imposed by the RD-1005-3 damper to find the range of the control voltage (±10 V) and the amplification gain equal to 1.2. Accordingly, the output voltage becomes ±12 V. Current intensity and voltage measurement can be taken at the output from the controller. The voltage measurement circuit ensures the adequate level of the voltage signal and protects the I/O card inputs. Current intensity measurements are taken with the Hall sensor [1]. The processing range of the sensor is ±5 A. The relationship between the output voltage from the sensor and the applied current is U_{hall}=2.5+0.185I_{out} (scaling 185 mV/A), where: U_{hall} – output voltage in the Hall sensor V, I_{out} – applied current A.

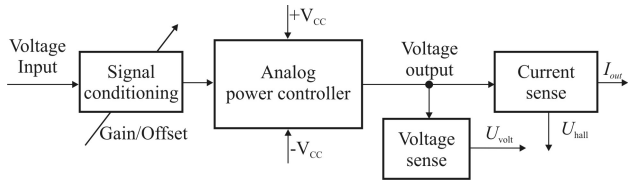

Fig. 2. Analog mode of the power controller
Rys. 2. Analogowy tryb pracy sterownika mocy

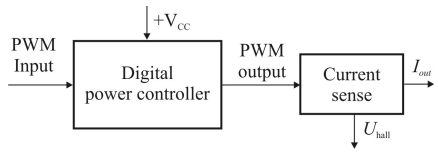

Fig. 3. Digital mode of the power controller
Rys. 3. Cyfrowy tryb pracy sterownika mocy

The structure of the power controller operating in the PWM digital mode utilizes integrated bridge circuits supported by control logic and protection system (Fig. 3). Measurements of the current level are taken with an integrated Hall sensor (LEM) incorporating the signal conditioning system (output current into voltage conversion and a voltage amplifier with the offset control). For the preset range of applied current (±5 A) the voltage signals becomes ±5 V.

The technical specification of the power controller (for a single channel) is provided in Table 1. In the analog mode the device offers: three power outputs, maximal output current of 3 A, supply voltage of ±15V (change of current direction is possible). In the digital mode it offers: three power outputs, maximal output current of 3 A (6 A in "peak" during 200 ms), supply voltage +12V (change of current direction is possible).

Tab. 1. Technical specification of the power controller
Tab. 1. Specyfikacja techniczna sterownika mocy

Parameter	Analog	Digital
DC supply voltage	(± 8, ± 30) V	(12, 55) V
Peak current	± 6 A	± 6 A (200 ms)
Max. continuous current	± 3 A	± 3 A
Range of external PWM frequency	NA	(5, 30) kHz
Recommended frequency (for user)	NA	(15, 30) kHz
Power dissipation at continuous current	30 W	25 W
Thermal protection	>170°C (shutdown)	>145°C (warning), >170°C (shutdown)
Shorted load protection	Yes	Yes
Current sensing	4 mA/A	377 µA/A

The power controller can operate in an open loop or closed-loop system. In the closed-loop system a current output of the power controller both in the analog and digital mode is provided (Fig. 4). Usually, for the controller with current output, a PI controller running on a PC or a microcontroller is applied. In the analog mode, the power controller regulates the voltage input and in the digital mode the duty cycle based on the error Δi [2]. The error Δi is the difference between the measured current i and the desired current i_0.

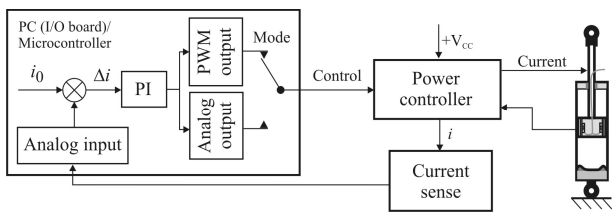

Fig. 4. Schematic of the power controller with current output
Rys. 4. Schemat sterownika mocy z wyjściem prądowym

2.2. Characteristics

The characteristics of the power controller were established by experimental tests run on a RD-1005-3 damper.

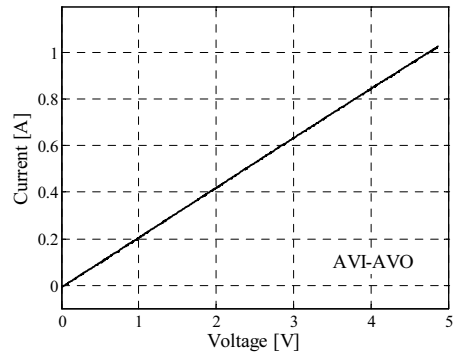

Fig. 5. Static characteristics in the analog mode
Rys. 5. Charakterystyka statyczna w trybie analogowym

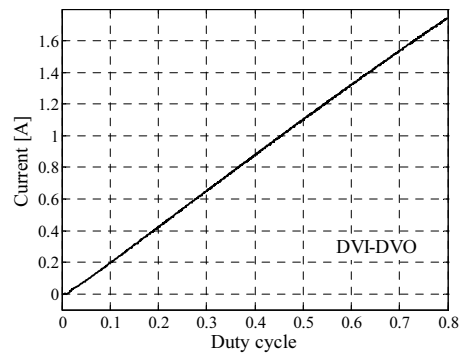

Fig. 6. Static characteristics in the digital mode
Rys. 6. Charakterystyka statyczna w trybie cyfrowym

Static characteristics were determined by measuring current at the device output in steady-state. The obtained static characteristics are shown in Figs 5–6. The plots in Fig. 5 show current vs. voltage in the analog mode (AVI–AVO) and in Fig. 6 current vs. duty cycle in the digital mode (DVI–DVO). It is readily apparent that the characteristics might be well approximated as linear.

Dynamic characteristics were determined by measuring the time of current stabilization in the coil and the force under the rapid change of the input signal (voltage or duty cycle). The RD-1005-3 damper was subjected to triangle displacement excitations with amplitude of 10×10^{-3} m and frequency of 1 Hz, and at the same time its electrical circuit was supplied by the controller. The measured quantities were: displacement excitation, input voltage, current response and force response. The obtained characteristics are provided in Figs 7−10. The plots in Figs 7–8 show current responses of the damper in the analog and digital mode, while the plots in Figs 9–10 present force responses of the damper in these two modes.

The obtained results reveal that the device dynamics for AVI–AVO and DVI–DVO might prove too slow when the current changes rapidly. That is of major importance when switching control algorithms are used. The substantial reduction of the damper current response time and thus force response time can be achieved for AVI–ACO and DVI–DCO.

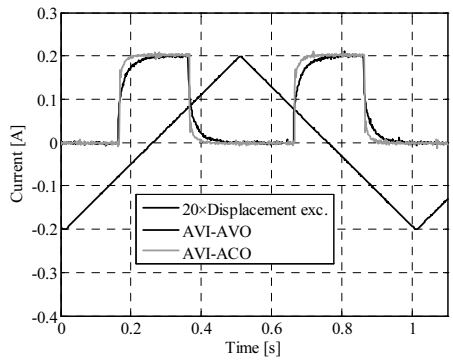

Fig. 7. Current responses in the analog mode
Rys. 7. Odpowiedzi prądowe w trybie analogowym

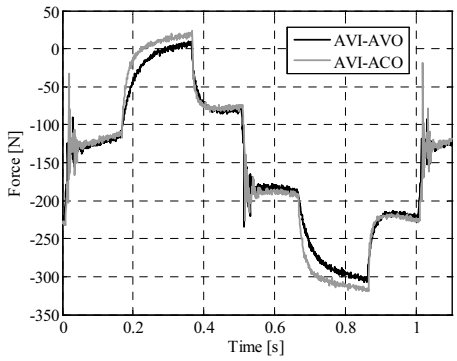

Fig. 8. Force responses in the analog mode
Rys. 8. Siły tłumienia w trybie analogowym

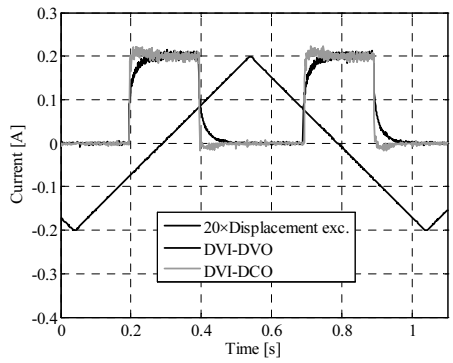

Fig. 9. Current responses in the digital mode
Rys. 9. Odpowiedzi prądowe w trybie cyfrowym

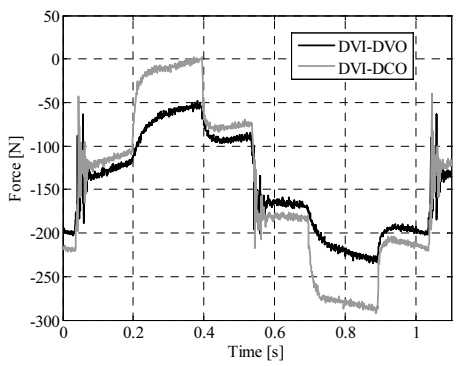

Fig. 10. Force responses in the digital mode
Rys. 10. Siły tłumienia w trybie cyfrowym

The plots in Figs 7−10 lead us to the following conclusions:
- the current response reached the steady state, both for AVI–AVO and DVI–DVO (and obviously for the device with current output),
- time to reach 95% of current final value was decreased when comparing AVI–AVO and DVI–DVO (open loop system) and AVI–ACO and DVI–DCO (closed-loop system),
- the force response did not reach the steady state for AVI–AVO and DVI–DVO,
- time to reach 95% of force final value for AVI–ACO was 0.182 s and for DVI–DCO it was 0.166 s,
- maximal difference value between force responses when comparing AVI–AVO and AVI–ACO was 13 N, while for DVI–DVO and DVI–DCO it was 50 N,
- maximal value of force achieved for AVI–ACO was 20 N, while for DVI–DCO it was –1.0 N.

3. Structures and control system of vehicle suspension model

The power controller was tested by using control of an MR damper in a vehicle suspension. model. The model was investigated as a structure with 2DOFs in the analog mode and with 3DOFs in the digital mode and that required to use two or three MR dampers of RD-1005-3 series [3].

3.1. Structure with two degree of freedom

In Fig. 11 we show the structure with 2DOFs where x is vertical displacement (bounce) and φ is longitudinal pitch with respect to P_g. The structure comprises a stiff beam (with height a and width b), with the mass m and the moment of inertia J with regard to beam's centre of gravity (cog) P_g, supported jointly at points P_f, P_r on identical spring-damper systems. The mechanical constraints of the structure motion are ensured with rigid stabilizing vertical guides positioned symmetrically on two sides of the beam (to restrict the motion of the beam's cog). The disturbances are designated by z_f, and z_r, springs stiffness in front and rear sections by k_f and k_r, and currents in the dampers by i_f and i_r, respectively. It is assumed that distance $l_f + l_r$ is large in relation to the maximal amplitude of vertical displacement x of the beam's cog. The numerical data of the investigated structures' parameters are listed in Table 2.

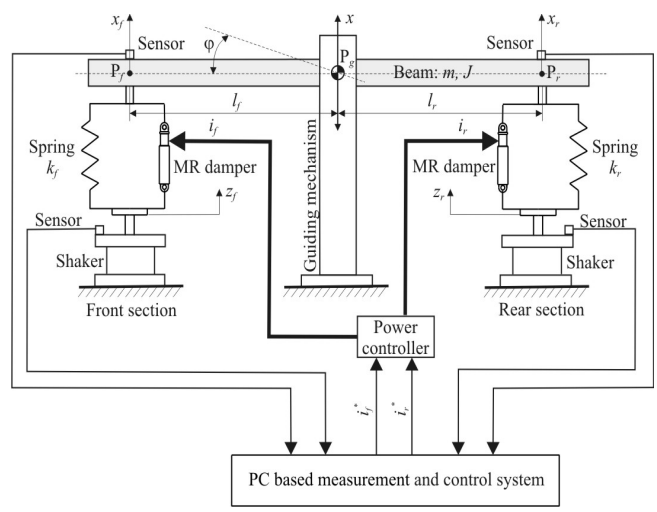

Fig. 11. Structure with 2DOFs
Rys. 11. Struktura o dwóch stopniach swobody

Tab. 2. Numerical data of the 2DOFs structures' parameters
Tab. 2. Wartości parametrów struktury o dwóch stopniach swobody

Parameter	Value
l_f	0.7 m
l_r	0.7 m
a	0.129 m
b	0.120 m
m	176.73 kg
m_s	66.73 kg
J	33.74 kgm^2
k_f	42016 N/m
k_r	42016 N/m

The schematic of the measurement and control system developed for the structure with 2DOFs is shown in Figure 12. The system is based on a PC with RT-DAC4 I/O board installed and the power controller operated in the analog mode. It is supported by software of Windows XP, MATLAB/Simulink and Real Time Workshop/Real Time Windows Target (RTW/RTWT). The control algorithm is implemented in the MATLAB/Simulink environment. The input signals are disturbances z_f, z_r and displacements x_f, x_r, and the output signal were currents i_f^* , i_r^* .

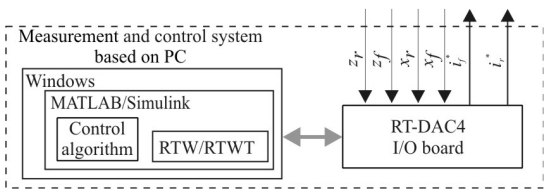

Fig. 12. Measurement and control system for the structure with 2DOFs
Rys. 12. Układ pomiarowo-sterujący dla struktury o dwóch stopniach swobody

In Fig. 13 we show a Simulink model that was used to build a real-time controller for the structure with 2 DOFs. This model utilizes analog inputs for displacement, voltage and current sensors (*RT-DAC Analog Inputs* block) and two analog voltage output channels (*RT-DAC PCI Analog Outputs* block) of the RT-DAC4/PCI I/O board. Signals from the *RT-DAC Analog Inputs* block are processed by the *Analog inputs processing* block into the linear positions x_f, x_r, z_f and z_r in meter unit, which are further utilized to generate control signals i_f and i_r (*Controller* block). Thus control signals are fed to the *Current Voltage RD-1005-3* block which convert control signals to the range of 0-10 V, since the control action uses analog voltage signals.

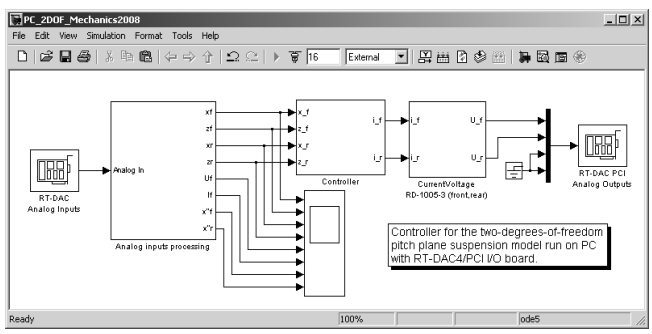

Fig. 13. Simulink diagram for the control system based on a PC with RT-DAC4 I/O board
Rys. 13. Diagram Simulinka dla układu sterowania z komputerem PC i kartą wejść-wyjść RT-DAC4

3.2. Structure with three degree of freedom

In Fig. 14 we show the structure with 3DOFs. In comparison to the structure with 2DOFs, this structure additionally consists of a rigid plate (modelling the driver and the seat/cab) of mass m_s and moment of inertia J_s with regard to plate's COG (P_s). The plate is suspended in P_g on spring-RD 1005-3 damper set. The spring stiffness is k_s, current in the damper is i_s and resistance force produced by the damper is F_{ds}. The plate motion is intended to be restricted to the direction perpendicular to the beam. The numerical data of the investigated structures' parameters are listed in Table 3.

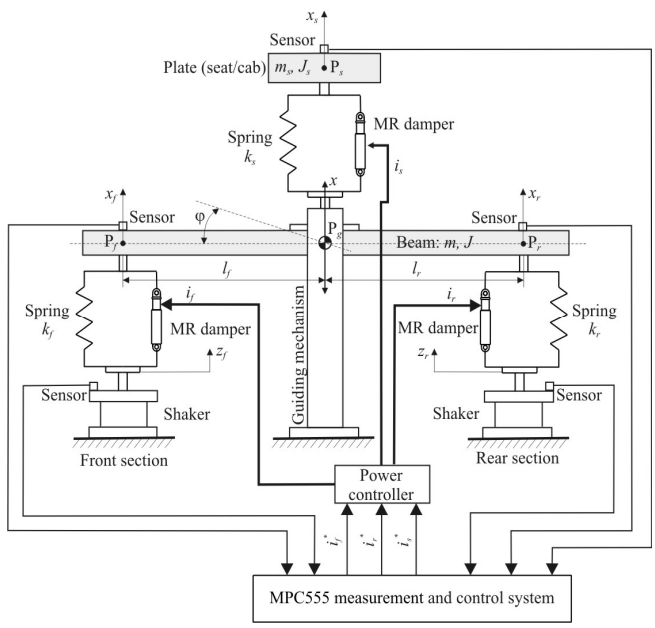

Fig. 14. Structure with 3DOFs
Rys. 14. Struktura o trzech stopniach swobody

Tab. 3. Numerical data of the 3DOFs structures' parameters
Tab. 3. Wartości parametrów struktury o trzech stopniach swobody

Parameter	Value
l_f	0.7 m
l_r	0.7 m
a	0.129 m
b	0.120 m
m	191.68 kg
m_s	66.73 kg
J	49.81 kgm^2
k_f	42016 N/m
k_r	42016 N/m
k_s	31565 N/m

The schematic of the control system developed for the structure with 3DOFs is presented in Fig. 15. The system utilizes the phyCORE-MPC555 single target board computer (with a MPC555 microcontroller) supported by the software environment installed on a PC. The power controller operates in the digital mode.

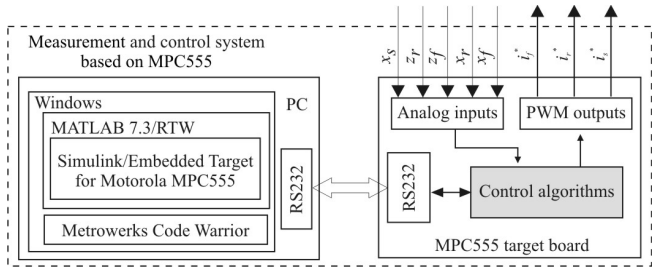

Fig. 15. Measurement and control system for the structure with 3DOFs
Rys. 15. Układ pomiarowo-sterujący dla struktury o trzech stopniach swobody

The applications available on phyCORE-MPC555 are activated from SRAM or FLASH-ROM. The architecture of the MPC555 microcontroller comprises [4]:
- 32-bit PowerPC core with 64-bit floating-point unit,
- 36 Kbytes fast RAM and 6 Kbytes TPU (Time Processor Unit) microcode RAM,
- 1 Mbyte flash EEPROM,
- three CAN 2.0B controller modules,
- 40 analog inputs: dual queued A/D converters with 10-bit resolution and typical conversion time of 5 μs,
- twelve 16-bit PWM module,
- multi-purpose I/O signals.

The PWM control signals for dampers are generated in the relevant digital outputs of the MPC555. The input-output data are acquired and monitored via the RS232 serial interface using a data acquisition and monitoring system based on PC.

The application for the MPC555 microcontroller, implemented in the MATLAB/Simulink environment, is generated in the real-time mode execution for rapid prototyping. These modes enable the use of the developed controller in Simulink to perform embedded control [5]. The real-time controller blocks contain the procedure for use of the key elements of the MPC555 microcontroller internal structure, supplied in the form of libraries with the toolbox Embedded target for Motorola MPC555. The feedback loop is closed by employing and input-output drivers (for sensors and actuators). This scheme is further utilized to generate and compile a C++ code. The resultant file, approved by MPC555, is downloaded to the microcontroller memory and activated accordingly.

In Fig. 16 we show Simulink diagram used to build a real-time controller for the structure with 3DOFs.

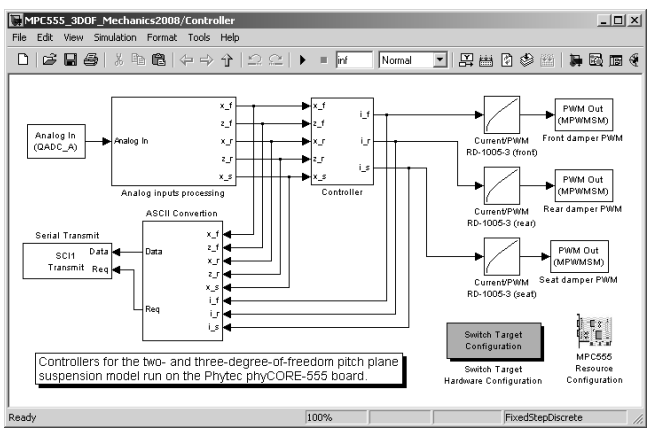

Fig. 16. Simulink diagram for the control system based on the MPC555 microcontroller target board
Rys. 16. Diagram w Simulinku dla układu sterowania z mikrokontrolerem MPC555

This model utilizes analog inputs for LVDT and laser sensors (*QADC_A* block), three PWM output channels (*MPWMSM* blocks) and a serial transmission module (*SCI1* block) on the phyCORE-MPC555 board. Signals from the *QADC_A* block are transmitted in the form of 16-bit digits to the *Analog inputs processing* block. These digits are then converted into the linear positions x_f, x_r, x_s, z_f and z_r in meter unit, which are further utilized to generate control signals i_f^*, i_r^* and i_s^* (*Controller* block). Thus control signals are fed to the *CurrentPWM* blocks which convert control signals to the range 0−1, since the control action uses PWM signals. The *MPC555 Resource Configuration* block allows us to examine, edit and set the MPC555 resource configuration. It is seen that the block is not connected to other blocks via input or output ports, however, it provides information to other blocks of the model.

4. Laboratory testing

The main purpose of tests was to prove the adequacy of generated output signals i_f, i_r (i_f, i_r, i_s) of the power controller. The displacements x_f, x_r (x_f, x_r, x_s) and disturbances z_f and z_r were measured by linear displacement transducers. In the digital mode the RD-1005-3 dampers were activated by PWM signals with frequency 30.0 kHz and in the analog mode by voltage in the range (0, 2.5) V. The sampling frequency was assumed to be 1 kHz. The range of control signals i_f^*, i_r^* (i_f^*, i_r^*, i_s^*) were established to be (0.00, 0.15) A [6].

4.1. Control algorithm

The control objective was to reduce vertical and angular accelerations of the beam for the structure with 2DOFs (and the seat for the structure with 3DOFs only). For this purpose a cascade algorithm based on the LQ control theory was applied. The schematic of the algorithm is shown in Fig. 17 [7]. It should be noted that the designations in brackets have to be taken into account only for the structure with 3DOFs. Two blocks are readily apparent in the schematic of the algorithm. The inputs to the first block are linear and angular velocities $\dot{x}$, $\dot{\varphi}$ (and $\dot{x}$ for the structure with 3DOFs only), and relative displacements Δx_f Δx_r (Δx_s). The outputs are optimal values of the dampers forces according to the LQ concept. The solution to the LQ problem: minimizes the quadratic performance index of the LQ controller [8]:

$$J = \int_0^\infty \left(x^T Q x + u^T R u + 2 x^T N u \right) dt \tag{1}$$

where: $\boldsymbol{X} = \left[\Delta x_f \quad \Delta x_r \quad \dot{x} \quad \dot{\varphi}\right]^T$, $\boldsymbol{X} = \left[\Delta x_f \quad \Delta x_r \quad \Delta x_s \quad \dot{x} \quad \dot{\varphi} \quad \dot{x}_s\right]^T$ are state vectors and $u = \left[F_{df}^* \; F_{dr}^*\right]^T$, $u = \left[F_{df}^* \; F_{dr}^* \; F_{ds}^*\right]^T$ are input (control) vectors for the structure with 2DOFs and 3DOFs respectively, and R are positively defined constant weighting matrices.

The second block implements the inverse model of the RD-1005-3 damper. An inverse model in the front (or rear) section translates the damper force F_{df}^* (or F_{dr}^*) determined for an instantaneous piston velocity $\dot{x}_f - \dot{z}_f$ (or $\dot{x}_r - \dot{z}_r$) into the value of the control current i_f^* (or i_r^*). The operation of the inverse model of seat damper is analogical. The inverse model was developed as the mapping ascribing the current in the damper coil to present damper force and piston velocity values. This mapping was based on measurements of the RD-1005-3 damper force taken under triangular base displacements with the amplitude 3.75×10^{-3} m and frequency range of (0.33, 8) Hz for currents in the range (0, 0.8) A.

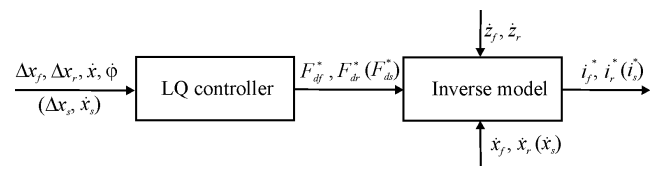

Fig. 17. Control algorithm
Rys. 17. Algorytm sterowania

4.2. Analog mode

Experiments for the structure with 2DOFs were conducted under double-sided sine base disturbances $z_f = z_r$ with amplitude 3.5×10^{-3} m and frequency in the range (1, 9) Hz. Results are shown in Figs 18−20.

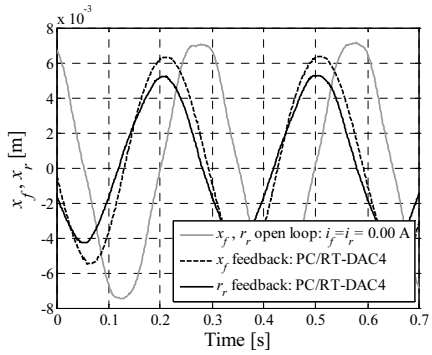

Fig. 18. Time patterns of displacements x_f and x_r
Rys. 18. Przebiegi czasowe przemieszczeń x_f i x_r

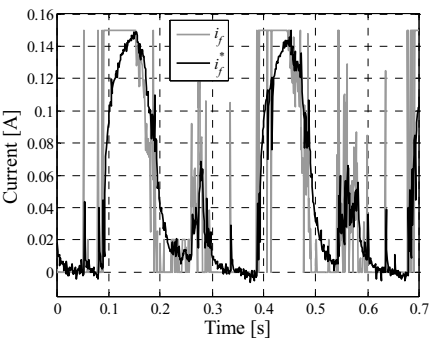

Fig. 19. Time patterns of currents i_f and i_f^*
Rys. 19. Przebiegi czasowe prądów i_f i i_f^*

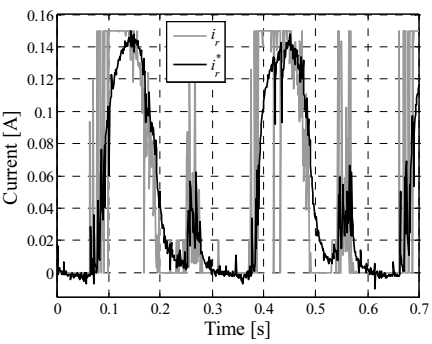

Fig. 20. Time patterns of currents i_r and i_r^*
Rys. 20. Przebiegi czasowe prądów i_r i i_r^*

Time patterns of displacements x_f and x_r acquired at frequency of about 3.5 Hz for the dampers in passive mode (0.00 A) with that in controlled mode are compared in Fig. 18. Time patterns of control signals generated by the control algorithm i_f^* and i_r^* with that measured in the dampers' coil i_f and i_r are compared in Figs 19−20. It is readily apparent that the parameters of the damper control circuit affect the current levels i_f and i_r. It is also observed that short pulses of control signals i_f^* and i_r^* are filtered, and measured signals i_f and i_r reached the steady state after the time approximately equal to the time constant of the damper control circuit.

4.3. Digital mode

The experiments for the structure with 3DOFs were conducted under double-sided sine base disturbances $z_f = z_r$ with amplitude 3×10^{-3} m and frequency in the range (1, 9) Hz. The results obtained for frequency of f=3.4 Hz (hence in the resonant range of the vertical motion) are shown in Figs 21−24.

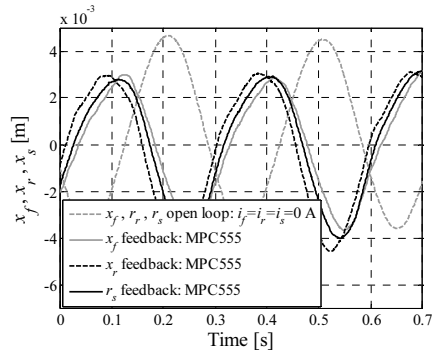

Fig. 21. Time patterns of displacements x_f, x_r and x_S
Rys. 21. Przebiegi czasowe przemieszczeń x_f, x_r i x_S

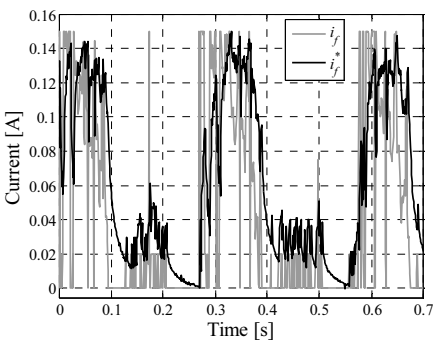

Fig. 22. Time patterns of currents i_f and i_f^*
Rys. 22. Przebiegi czasowe prądów i_f i i_f^*

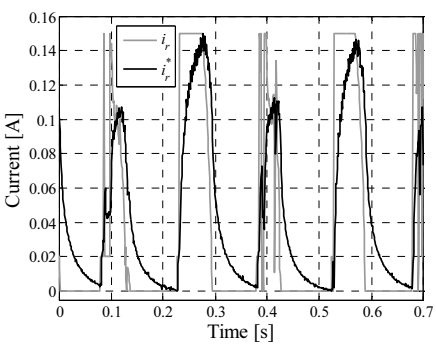

Fig. 23. Time patterns of currents i_r and i_r^*
Rys. 23. Przebiegi czasowe prądów i_r i i_r^*

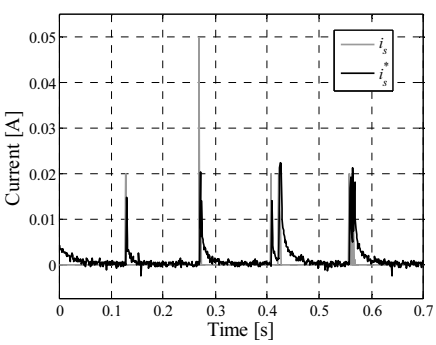

Fig. 24. Time patterns of currents i_s and i_s^*
Rys. 24. Przebiegi czasowe prądów i_s i i_s^*

Time patterns of displacements x_f, x_r, and x_s for the dampers in the passive mode with that in controlled mode are compared in Fig. 21. It is apparent that the dampers in controlled mode provide

vibration reduction in the resonant zone both in terms of vertical motion and longitudinal pitching.

Time patterns of control signals generated by the control algorithm i_f^*, i_r^* and i_s^* with that measured in the dampers' coil i_f, i_r and i_s are compared in Figs 22−24. Similarly to controllers operating in the analog mode, parameters of the of the damper control circuit affect the current levels i_f, i_r and i_s.

5. Summary

The paper presents the power controller for small-scale MR dampers. The structure, technical specification, characteristics and results of laboratory tests of the device by applying to MR dampers' control in a vehicle suspension model. The device was tested in the analog and digital mode in a structure with 2DOFs and 3DOFs respectively.

The power controller enables us to simplify the wiring structure and change the current flow direction. The latter is an important problem for demagnetization algorithms. Besides, the digital mode enables the power controller to be directly connected to the digital outputs of the control system (microcontroller, I/O board) without D/A converters. Easy adjustment of supply voltage, selection of the PWM signal frequency in a broad range and generation of maximal current levels (5−6) A make it an good tool for the controlling any small-scale MR damper.

Results of the conducted tests prove the adequate performance of the power controller operation in the analog and digital mode.

This work is supported by AGH University of Science and Technology under research program No. 11.11.130 (2009).

6. References

[1] Allegro MicroSystems Inc.: ACS712. Fully Integrated Hall Effect-Based Linear Current Sensor, Technical documentation, Rev. 9, (2009).
[2] Rosół M., Sapiński B.: Dynamics of a Magnetorheological Damper Driven by a Current Driver. Proc. of the 12th IEEE Int. Conf. on Methods and Models in Automation and Robotics, Poland (2006), 423–428.
[3] Lord Corp.: RD-1005-3 damper. Technical data, http://www.lord.com (2006).
[4] Motorola Corporation: MPC555/MPC556 User's Manual. USA (2000).
[5] The MathWorks Inc.: Embedded Target for Motorola MPC555. User's Guide. Ver. 2. USA (2005).
[6] Rosół M., Sapiński B.: Power controller for small – scale magnetorheological dampers", Proc. of the IV Eccomas Thematic Conference on Smart Structures and Materials, 13-15 July, Porto, Portugal, (2009).
[7] Martynowicz P., Sapiński B.: Experimental study of vibration control in a two-degree-of-freedom pitch-plane model of a magnetorheological vehicle suspension", Quarterly Mechanics, AGH University of Science and Technology Press, Cracow, Vol. 26, 60–70 (2007).
[8] Lublin L., Athans M.: Linear Quadratic Regulator Control. The Control Handbook, Library of Congress Cataloging-in-Publication Data, CRC Press in Cooperation with IEEE Press (1996), 635–650.

otrzymano / received: 07.10.2009
przyjęto do druku / accepted: 03.02.2010 *artykuł recenzowany*

INFORMACJE